Journal of Applied Fluid Mechanics, Vol. 13, No. 3, pp. 1027-1035, 2020.
Available online at www.jafmonline.net, ISSN 1735-3572, EISSN 1735-3645.
DOI: 10.29252/jafm.13.03.30626

Resistance Force on a Spherical Intruder in Fluidized Bed

A. A. Zaidi

School of Mechanical and Manufacturing Engineering, National University of Sciences & Technology H-12, Islamabad, 44000, Pakistan

†*Corresponding Author Email: ali.zaidi@smme.nust.edu.pk*

(Received June 15, 2019; accepted October 15, 2019)

ABSTRACT

Insertion of large objects or intruders into granular material is common both in nature and industrial applications. During penetration due to collision between intruder and granular particles, intruder experiences resistance or drag force (analogy from fluid). In literature, it is extensively studied that in dry packed beds granular drag force increases with the intrusion depth. However, nearly no information is available about the effect of fluidization on the granular drag force and is the main theme of this paper. In this paper, discrete element method (DEM) and computational fluid dynamics (CFD) is used for performing numerical simulations. Simulations showed that granular drag force becomes independent of intrusion depth at incipient fluidization and is a function of Reynolds number. Using the mathematical relation of fluid drag force, granular viscosity of the fluidized bed is calculated. The physics for the fluid like state of granular material and the independence of granular drag force with intrusion depth is explained at the end of paper.

Keywords: Resistance force; Fluidized bed; Intruder impact; Granular viscosity; Discrete element method.

NOMENCLATURE

A	characteristics area
Ar	Archimedes number
c	exponential fitting parameter
C_d	drag coefficient
D	intruder diameter
d_p	diameter of particles
f	friction coefficient
$\boldsymbol{f}_p$	drag force in volume averaged equation
$\boldsymbol{f}_{pI}$	forcing function in IBM
$\boldsymbol{F}_n$	normal contact force on particle
$\boldsymbol{F}_t$	tangential contact force on particle
$\boldsymbol{F}_{fI}$	fluid force acting on intruder
F	granular drag force
F_{fluid}	fluid drag force
$F(z)$	depth dependent hydrostatic component of granular drag force
$F(v)$	velocity dependent viscous component of granular drag force
F_0	frictional component of granular drag force
F_{mag}	magnitude of fluid drag force
g	gravity
G_t	relative particle velocity between particles during collision in tangential direction
$\boldsymbol{G}$	relative particle velocity between colliding particles
k	fitting parameter
K	spring constant
K_t	tangential spring constant]
K_n	normal spring
m	mass of particle
$\boldsymbol{M}_{fi}$	fluid moment acting on intruder
$\boldsymbol{n}$	normal unit vector at the contact point
p	fluid pressure
Re_{mf}	Minimum fluidization velocity Reynolds number
$\boldsymbol{r}$	radius of intruder
$\boldsymbol{t}$	tangential unit vector at the contact point
U	fluidization velocity
$\boldsymbol{u}$	fluid velocity in volume averaged equation
$\tilde{\boldsymbol{u}}$	volume weighted fluid velocity by IBM
U_{mf}	minimum fluidization velocity of the bed
v	intrusion velocity
$Vp1$	volume of cube enclosing all sides of intruder
$\boldsymbol{v}_p$	particle velocity
$\boldsymbol{V}_I$	intruder velocity
W_{avg}	average weight of particles in hemisphere
z	intrusion depth
ρ_g	fluid density
ν	kinematic viscosity
μ_f	fluid viscosity
μ_g	granular viscosity
α	solid volume fraction of intruder in fluid grid cell
β	drag coefficient
ε	void fraction in fluid grid cell
φ	packing fraction

η_t	tangential damping coefficient	δ_n	overlap in normal direction
η_n	normal damping coefficient	Δt	time step
δ_t	overlap in tangential direction	Δx	fluid grid cell

1. INTRODUCTION

Granular material consists of large agglomerates of discrete particles. Under normal atmospheric conditions, the forces between granular grains are repulsive and the granular material takes the shape of container (Jaeger *et al.*, 1996). One of the distinct characteristics of granular material is that under different operating conditions i.e. vibration, fluidization, rotation etc. granular material transforms into different states of matter. For example: granular material acts as solid in large heap of sand, liquid in sand clock and gas in sand storm. Due to its unique properties, granular material can be classified as an additional form of matter. In this paper, the liquid state of granular material is discussed.

In fluidization, depending upon the gas velocity granular material changes to different intermediate states (Yang, 2003). For smaller gas velocity, the particles do not move and the bed remains packed due to weak fluid drag acting on particles and the pressure drop across the bed increases with the increase in gas velocity. By further increase in gas velocity, at certain critical point, the fluid drag becomes nearly equal to particles weight. At this point, the bed expands and the pressure drop across the bed becomes constant with further increase in gas velocity. Any further increase in gas velocity results in bubble formation in granular material and finally leads to pneumatic conveying of granular particles. In this paper, granular material near to incipient fluidization is studied for the calculations of granular drag force.

In literature, there are various problems that are studied for granular material (Le Guen *et al.* 2011). For example: segregation (Ottino & Khakhar 2000) and jamming of granular material under shear (Behringer, 2015), fluidization (Nirmala & Muruganandam 2015), Taylor vortices formation in granular particles (Conway *et al.* (2004)) etc. One particularly interesting problem is the insertion of intruder or large object into granular material and calculation of resulting resistance or granular drag force. It has various applications both in nature and industry e.g. crater formation by meteors and projectiles, foot and tire prints on sand, lifting of soil using tractor blades, bullet penetration in sand bag etc. (Walsh *et al.* (2003); Uehara *et al.* (2003); Crassous *et al.* (2007); Clark *et al.* (2012)).

There are number of studies in literature; for modeling granular drag or resistance force acting on intruder. For example: Lohse *et al.* (2004) studied impact force acting on sphere by falling under gravity on sand and proposed that granular drag force increases linearly with the depth of intrusion. Peng *et al.* (2009) and Hill *et al.* (2005) observed power-law behavior of granular drag force with the depth of intrusion (with exponent=1.3). For intruders with relatively larger intrusion velocities; Katsuragi and Durian (2007) and Hou *et al.* (2005) proposed that besides the depth dependent term for modeling granular drag force there should also be another term which is a function of intrusion velocity. Hill *et al.* (2005) and Clark *et al.* (2014) investigated variation of granular drag force by changing shape of intruder. Besides the calculation of granular drag force, in literature there are also some studies related to tracking of motion of intruder in fluidized bed. For example: Lim and Agarwal (1994) studied circulation patterns around large sphere in two dimensional fluidized bed using experiments. Rios *et al.* (1986) studied the sinking and rising of large sphere by bubbles in fluidized bed.

In literature, thus reasonable studies are done for the motion of large objects both in packed and fluidized bed. However, in literature according to authors' knowledge variation of granular drag force on intruder in partially fluidized bed needs further investigation (at which the bed is neither perfectly packed nor fluidized) and covered in this paper.

2. FORMULATION

2.1 Particle-Particle Interactions

In simulations, for particle-particle and particle-intruder calculations soft sphere discrete element method (DEM) proposed by Cundall and Strack (1979) is used. Since this study involves granular particles and intruder of different sizes, thus DEM is explained by taking into account both events i.e. particle-particle collision and particle-intruder collision. Both events are shown in Fig. 1.

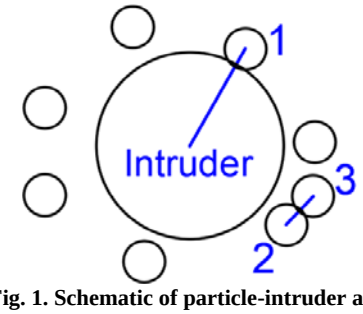

Fig. 1. Schematic of particle-intruder and particle-particle collision.

Since intruder and particles used in simulations are spherical in shape thus there is no difference in DEM calculations for modeling particle-particle (shown by particle 2 and 3 in Fig. 1) and particle-intruder collision (shown by particle 1 and intruder in Fig. 1). In DEM, first the neighboring particles are detected by particle in cell method (Sulsky *et al.* 1995) by using grid larger in size than the intruder diameter. Particle-particle collision is detected when the inter-particle distance is less than the sum of particles

radii. Similarly, particle-intruder collision is detected when the distance between intruder and particle is less than the sum of radii of particle and intruder. Then the overlap (δ) is calculated by taking the difference between sum of particles radii and inter-particle distance (in case of particle-particle collision) or by taking the difference between sum of particle and intruder radii with the inter-particle and intruder distance (in case of particle-intruder collision). The inter-particle and particle and intruder collision force is modeled by assuming the collision as friction slider, linear spring and dashpot as shown in Fig. 2.

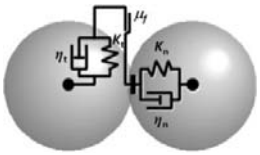

Fig. 2. Schematic of DEM model.

Furthermore, the collision or contact force is resolved into tangential F_t and normal components F_n modeled by Eq. (1) and (2) respectively. If the magnitude of tangential force is larger than the product of friction coefficient and magnitude of normal force than slipping occurs and the tangential force is calculated by Eq. (4).

$$\boldsymbol{F}_t = (-K_t\delta_t - \eta_t G_t)\,\boldsymbol{t} \tag{1}$$

$$\boldsymbol{F}_n = (-K_n\delta_n - \eta_n \boldsymbol{G}\cdot\boldsymbol{n})\boldsymbol{n} \tag{2}$$

$$\text{If } |\boldsymbol{F}_t| > f|\boldsymbol{F}_n| \tag{3}$$

$$\boldsymbol{F}_t = -f|\boldsymbol{F}_n|\boldsymbol{t} \tag{4}$$

One more important point about DEM is the numerically stability. For stable DEM solution, time step during simulations should be smaller than one by tenth of the period of natural oscillations of a mass-spring system ($2\pi\sqrt{K}$). Thus, for numerically stability, simulations are run at a time step equal to 10^{-6} seconds.

2.2 Fluid-Particle Interactions

Simulations involve particles of the order $\backsim 10^5$. Thus, for reducing computational time and without compromising the reliability of results, locally phase-averaged Navier-Stokes equations (Anderson & Jackson 1967) are used in which fluid mesh is larger in size than particles and drag correlations are used for incorporating particle-fluid interactions. The details about fluid solver can be found somewhere else (Tsuji *et al.* 1993). The continuity and momentum equation of fluid are solved using SIMPLE (Patankar, 1980) and are given by:

$$\frac{\partial}{\partial t}\varepsilon + \nabla\cdot(\varepsilon\boldsymbol{u}) = 0 \tag{5}$$

$$\frac{\partial}{\partial t}(\varepsilon\boldsymbol{u}) + \nabla\cdot(\varepsilon\boldsymbol{u}\boldsymbol{u}) = -\frac{\varepsilon}{\rho_g}\nabla p + \varepsilon\nu\nabla^2\boldsymbol{u} + \boldsymbol{f}_p \tag{6}$$

$\boldsymbol{f}_p$ in Eq. (6) incorporates the particle effects on fluid. In this paper, the relation proposed by Zaidi (2018) is used in the calculation of β.

$$\boldsymbol{f}_p = \beta\frac{(\boldsymbol{v}_p - \boldsymbol{u})}{\rho_g} \tag{7}$$

Simulations involve intruders of diameter (D) which is either equal to or larger than six times particle diameter (d_p). However, in solving volume averaged equations fluid mesh should be 2-5 times larger than diameter of particle. Thus, immersed boundary method (IBM) is used for coupling intruder with fluid. In this paper only main points are discussed, details about this method can be found somewhere else (Zaidi, 2018; Zaidi *et al.* 2015). For coupling fluid with both particles and intruder same fluid grid size is used and only the fluid grid regions occupied by intruder are solved using IBM. Furthermore, at the interface of fluid and intruder, local grid refinement is used for the calculation of α and shown in the enlarged view in Fig. 3. (more details can be found in Zaidi (2018))

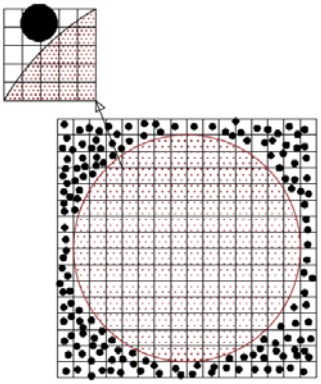

Fig. 3. Fluid grid in IBM.

After obtaining the volume weighted fluid velocity ($\boldsymbol{u}$). $\boldsymbol{u}$ is changed to $\tilde{\boldsymbol{u}}$ around intruder by linear interpolation and given by:

$$\tilde{\boldsymbol{u}} = \alpha\boldsymbol{V}_1 + (1-\alpha)\boldsymbol{u} \tag{8}$$

where α changes from zero to one for fluid and intruder grid cell respectively. The motion of intruder changes the value of α in the fluid grid cell which negligibly affect the numerical stability which is primarily dependent on the Courant number ($\tilde{\boldsymbol{u}}\Delta t/\Delta x$) for fluid calculations. After calculation of $\tilde{\boldsymbol{u}}$ forcing term ($\boldsymbol{f}_{pI}$) is calculated and given by Eq. (9).

$$\boldsymbol{f}_{pI} = \alpha\frac{(\boldsymbol{V}_I - \boldsymbol{u})}{\Delta t} \tag{9}$$

The volume integral of forcing term ($\boldsymbol{f}_{pI}$) is used for the calculation of fluid force and moment on intruder and given by Eq. (10) and (11) respectively.

$$\boldsymbol{F}_{fI} = -\rho_g\int_{Vp1}\boldsymbol{f}_{pI}dv \tag{10}$$

$$\boldsymbol{M}_{fI} = -\rho_g\int_{Vp1}\boldsymbol{r}\times\boldsymbol{f}_{pI}dv \tag{11}$$

It is to be noted that both total fluid force on particles and intruder and total force due to particles and intruder interactions are calculated independently. After calculation of net force, velocity and displacement of particles and intruder are obtained by integrating net acceleration.

3. SIMULATION SETUP

Simulations are done for cubic domain with walls to mimic cubical container. Random particle arrangement is obtained by giving the particles initial random velocity and let them settle under gravitational force using DEM solver only. The initial setup of simulation and size of computational domain are shown in Fig. 4.

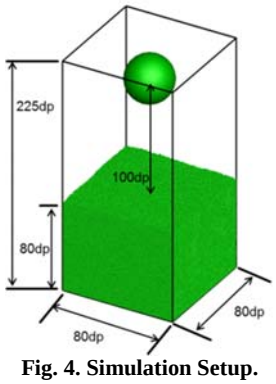

Fig. 4. Simulation Setup.

There are 512,000 particles in the computational domain and each and every particle is tracked during simulation. Glass particles are used in simulations with size, density, coefficient of restitution, coefficient of friction equal to 0.5 mm, 2500 kg/m^3, 0.65 and 0.2 respectively (Ishibashi *et al.* 1994; Sondergaard *et al.* 1990).

In simulations fluid grid is 2.5 times the particle diameter and the fluidizing medium is air. Similar approach for fluid grid selection was previously used by Li and Li (2018) and Li *et al.* (2017). The minimum fluidization velocity of air is calculated by simulations and compared with the relation of Wen and Yu (1966) given by:

$$U_{mf} = \frac{Re_{mf}\nu}{d_p} \tag{12}$$

$$Re_{mf} = (33.7^2 + 0.0408Ar)^{1/2} - 33.7 \tag{13}$$

$$Ar = \frac{{d_p}^3 \rho_g(\rho_g - \rho_p)g}{\mu^2} \tag{14}$$

The percentage difference between simulation results and Eq. (12) remains less than 10%. For calculation of granular drag force, intruder penetrates into granular material with constant velocity. In simulations, three parameters are studied i.e. intruder diameter, intruder velocity and degree of fluidization and their ranges are given in table 1. The second column in table 1 shows the parameters that are changed for each case while the parameters which are kept constant (for that case) are shown in column three and four.

4. RESULTS AND DISCUSSIONS

4.1 Drag force on intruder without fluidization of granular material

The main aim of this sub-section is to benchmark the simulation code by calculating the granular drag force in packed bed. In literature (Lohse *et al.* 2004); Katsuragi and Durian 2007; Xu *et al.* 2014), this problem is reasonably studied and the relation for modeling granular drag force can be written as:

$$F(Z, v) = F(z) + F(v) + F_0 \tag{15}$$

Table 1 Cases studied in simulations

Case 1	D/d_p=12,16, 20, 24	V_I=0.1 m/s	U/U_{mf}= 0
Case 2	V_I=0.1,0.2,0.3, 0.4 m/s	D/d_p=16	U/U_{mf}= 0
Case 3	U/U_{mf}=0,0.25, 0.5,0.75,1,1.25, 1.5,2	D/d_p=16	V_I=0.1 m/s
Case 4	D/d_p =12,16, 20, 24	U/U_{mf}=1. 25	V_I =0.1 m/s
Case 5	V_I=0.1, 0.3, 0.4 m/s	U/U_{mf}=1. 25	D/d_p = 16

In some work, F_0 is included in $F(z)$ rather than as a separate term (Katsuragi & Durian 2007). For intruders with relatively smaller velocities (i.e. $V_I \leq 0.8$ m/s, $F(v)$ can be neglected and $F(z)$ is generally written as shown in Eq. (14). (this value of V_I for ignoring $F(v)$ and the relation for $F(z)$ in Eq. (14) are obtained from literature (Lohse *et al.* 2004; Katsuragi & Durian 2007; Xu *et al.* 2014; Hou *et al.* 2005; Hill *et al.* 2005)

$$F(z) = kZ^c \tag{16}$$

Lohse *et al.* (2004) proposed the value of k=13.3 $\pm$0.5 N/m and c=1 using experiments of free fall of large object in loosely packed sand. Hill *et al.* (2005) using the plunging and retraction experiments of intruders into granular material proposed the value of k=15 $\pm$3 N/m and c=1.3.

The cases studied in this section are given by case 1 and case 2 in table 1. Figures 5 and 6 show the log-log plot of granular drag force as a function of intrusion depth for different intruder diameters and intrusion velocities respectively. The depth of intrusion is non-dimensionalized by the intruder diameter. The granular drag force is plotted after the intruder is fully submerged into granular material and before the granular drag force increases exponentially due to jamming of particles from the bottom surface (Stone *et al.* 2004).

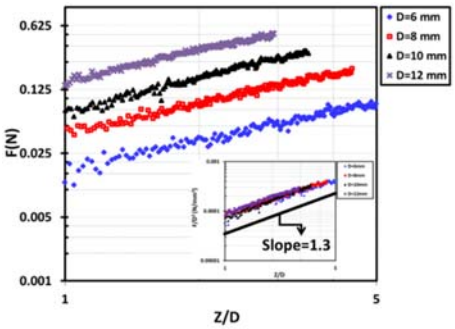

Fig. 5. Drag force F on intruder with different intruder sizes for V_I= 0.1 m/s and U/U_{mf} = 0 m/s.

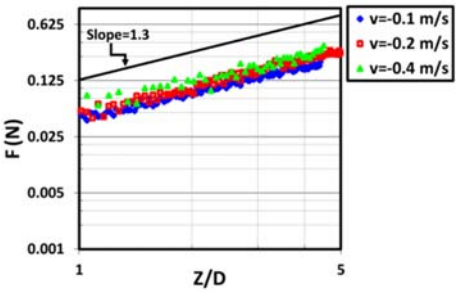

Fig. 6. Drag force F on intruder with different intruder velocities for D/d_p=16 and U/U_{mf} = 0 m/s.

It can be seen that the granular drag force increases with the diameter of intruder and remains independent with intrusion velocities (which is consistent with the low speed intruder dynamics). Furthermore, the granular drag force follows a power-law function of intrusion depth as was mentioned in Eq. (14). In the small inset in Fig. 5, the granular drag force is non-dimensionalised by the intruder volume. The non-dimensionalized granular drag force collapses on a single line for intruders of different diameters with a slope equal to 1.3 which is consistent with the findings of Hill *et al.* (2005).

4.2 Drag Force on Intruder in Fluidized Bed

In simulations for cases of fluidized bed, the fluid drag acts on both particles and intruder. However, since this paper in only focused on resistance force acting on intruder due to granular medium or granular drag force only this particular force is plotted in rest of figures. The cases studied in this section are given by case 3, 4 and 5 in table 1. Granular drag force is calculated for different fluidization velocities (U) and given in Fig. 7. U_{mf} in Fig. 7 is the ratio of U to U_{mf}.

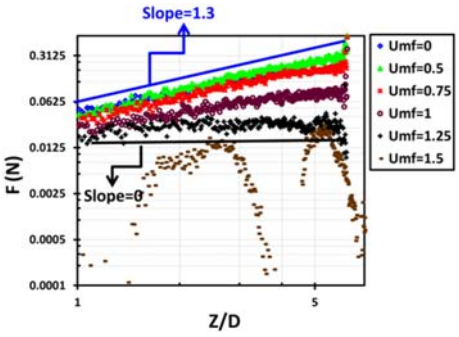

Fig. 7. Drag force F on intruder with different fluidization velocities for D/d_p=16 and V_I= 0.1 m/s.

It can be seen that the slope and the y-intercept of the granular drag force decreases with the increase in degree of fluidization especially after $U_{mf} > 0.75$. The slope of granular drag force approaches to zero with intrusion depth for U_{mf}=1.25 and becomes fluctuating for U_{mf}=1.5. The main reason for the fluctuations in granular drag force for U_{mf}=1.5 is bubble formation in fluidized bed. As the bubble rises near to intruder it develops void around intruder and thus reduces the granular drag force. After the bubble leaves the intruder, granular drag force increases again. This motion of bubbles develops fluctuations in granular drag force. The zero slope for U_{mf}=1.25 represents an interesting phenomenon and is further investigated.

For U_{mf} =1.25, the granular drag force becomes nearly independent of the intrusion depth which is a characteristics of fluid. In literature, the fluid drag force on a sphere is a function of relative velocity between fluid and sphere, sphere diameter and properties of fluid. But the fluid drag force has no dependence on the position of sphere in the fluid. For U_{mf} = 1.25, the effect of intruder diameter and intruder velocity on granular drag force is shown in Figs. 8 (a) and (b) respectively. Furthermore, it can be seen from Fig. 8 (b) that the granular drag force increases with the increase in intrusion velocity which was not present in the case of packed bed.

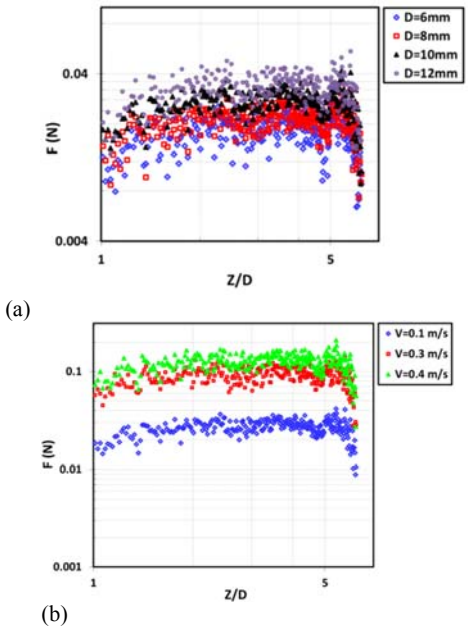

Fig. 8. Drag force F on intruder for Umf = 1.25 (a) Effect of intruder diameter at V_I= 0.1 m/s (b) Effect of intrusion velocity at D/d_p=16.

For better understanding, the normalized average granular drag force is plotted as a function of intruder diameter and intruder velocity in Figs. 9 (a) and (b) respectively at U_{mf} = 1.25. A linear relationship between the granular drag force and intruder diameter and intruder velocity can be seen.

For Newtonian fluids (e.g. air or water), drag force (F_{fluid}) due to fluid can be written as:

$$F_{fluid} = \frac{1}{2} C_d \rho_g A V_I^2 \quad (17)$$

Using drag correlation proposed by Schiller and Naumann (1935) for calculating drag coefficient and using intruder diameter for the calculation of A (i.e.

$A = \pi/4\, D^2$), Eq. (17) becomes:

$$F_{fluid} = 3\pi\mu_f D V_I (1 + 0.15Re^{0.687}) \quad (18)$$

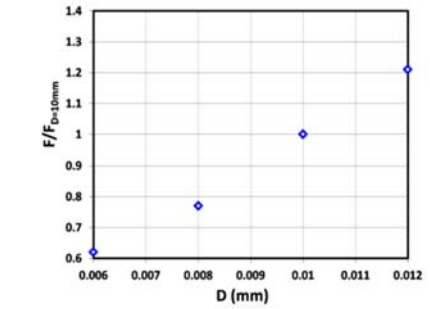

(a)

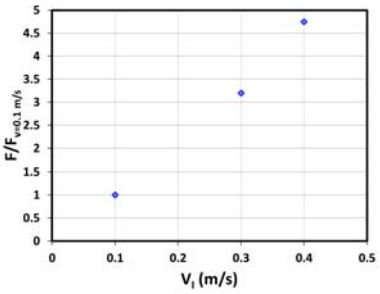

(b)

Fig. 9. Drag force *F* on intruder for Umf = 1.25 (a) as a function of intruder diameter at V_I= 0.1 m/s (b) as a function of intrusion velocity and D/d_p=16.

If we use the same analogy and assume granular material in fluidized state as complex fluid and replace μ_f to μ_g then we can calculate granular viscosity (μ_g). Similarly, Reynolds number of intruder during immersion in granular material Re can be calculated by:

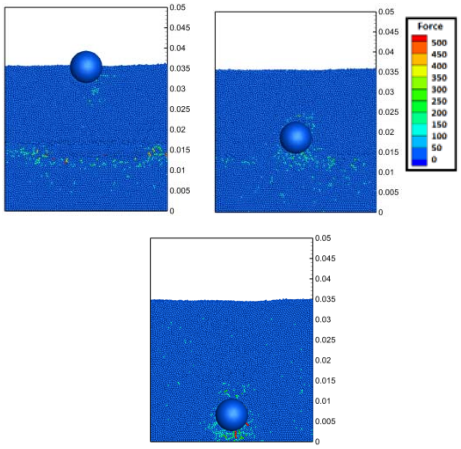

Fig. 11. Absence of force chains in fluidized bed during insertion of intruder. The force on particles is non-dimensionalized with the weight of particles.

$$Re = \frac{\rho_e D V_I}{\mu_g} \quad (19)$$

ρ_e is the effective density of granular material and can be obtained by $\rho_e = \rho_s \varphi$. where φ is the packing fraction. μ_g can be obtained as a fitting parameter by fitting the data for *F* as a function of Re (shown in Fig. 10).

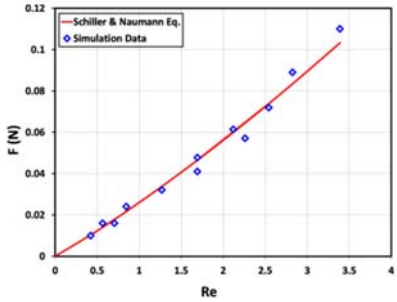

Fig. 10. Granular drag force on intruder as a function of Reynolds number.

The value of μ_g obtained by fitting is 1.695 Pa-s. The obtained value of granular viscosity is closer to the range proposed by Grace (1970) (0.4-1.3 Pa-s) using experiments in bubbling fluidized beds and also closer to the range proposed by Schugerl *et al.* (1961) (1.2-5 Pa-s) using Couette-type viscometer for fluidized bed. However, μ_g from simulations deviates significantly from the simulation results of Xu *et al.* (2014) (0.2 Pa-s). It can be due to calculation of granular viscosity for partially submerged intruder in packed bed by Xu *et al.* (2014).

4.3 Physics behind the variation of drag force with fluidization

In Subsection 4.2, we have seen that the simulation data for U_{mf} = 1.25 fits well with the fluid drag correlation. Thus, it can be inferred that at fluidization, the granular material loses it solid like properties and behaves more like a fluid. For further elaborating this point, in Figs. 11 and 12 the snapshots of insertion of intruder (D/d_p=16) are shown in packed and fluidized bed (U_{mf} = 1.25) at the center slice of computational domain. The color of particles shows the magnitude of resultant force (F_{mag}) acting on particles non-dimensionalized by the weight of particles.

$$F_{non-dim} = \frac{F_{mag}}{mg} \quad (20)$$

The force network or chains of particles show the resistance force experienced by intruder during penetration into granular material. The larger is the size of force chains below intruder, the larger will be resistance or granular drag force. It can be seen from Figs. 11 and 12; the force chain network below the surface of intruder is stronger in case of packed bed. Furthermore, in packed bed as the intrusion depth increases the strength of force chain network also increases. However, for fluidized bed clear force chain network is not present regardless of intrusion depth.

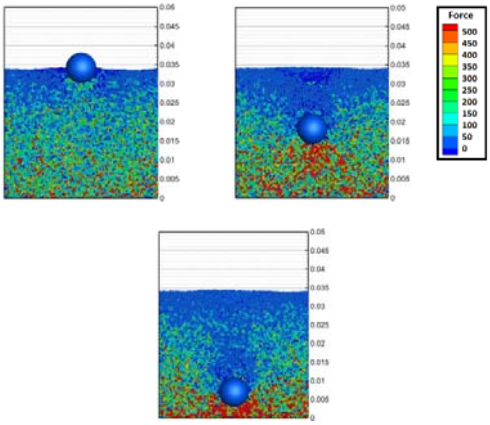

Fig. 12. Formation of force chains in packed bed during insertion of intruder. The force on particles is non-dimensionalized by the weight of particles.

Furthermore, in Fig. 11 it can be seen that the bed height is larger in fluidized bed in comparison with packed bed in Fig. 12. This is due to passing of gas through the bed which decreases the packing fraction and makes the bed loosely packed. As the grains are relatively further apart in case of fluidized bed and their weight is counterbalanced by the fluid drag force. Thus, when the intruder immerses into granular material the local increase in packing fraction and corresponding force network around intruder with the increase in intrusion depth does not happen. This results into depth independent granular drag force with intrusion depth in fluidized bed which is similar to conventional fluids. However, in case of packed bed due to increase in local packing fraction around intruder with the depth of intrusion results in formation of stronger force chains and increase in granular drag force with intrusion depth.

For further understanding, the average granular drag force on particles below the intruder surface is calculated in an imaginary hemisphere (concentric with intruder) with radius two times the intruder radius for both packed and fluidized bed (U_{mf} = 1.25) and shown in Fig. 14. The schematic diagram is shown in Fig. 13.

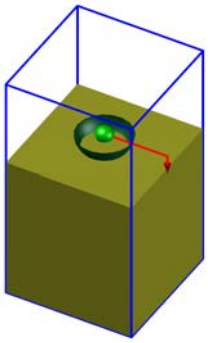

Fig. 13. Imaginary hemisphere for calculation of local granular drag force on intruder.

It can be seen in Fig. 14 that for packed bed the average granular drag force keeps increasing with the depth of intrusion and for fluidized bed the granular drag force becomes independent with the intrusion depth as was observed previously.

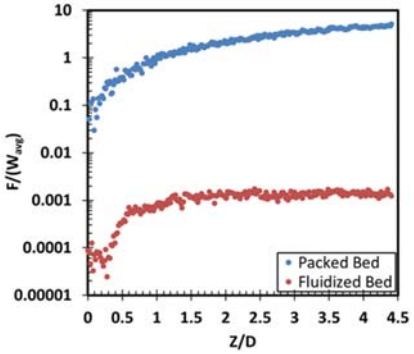

Fig. 14. Average granular drag force on particles in an imaginary hemisphere.

5. CONCLUSION

Simulations are performed for calculations of granular drag force in packed and fluidized bed. In packed bed, simulations showed that granular drag force is a function of intrusion depth and can be modeled using power-law i.e. $F = kz^{1.3}$ in agreement with literature results. For fluidized bed, it is observed that fluidization decreases the granular drag force. At 1.25 times the minimum fluidization velocity, granular drag force becomes nearly constant with the intrusion depth and behaves more like a fluid. In this condition, the fluid correlation i.e. one proposed by Schiller and Naumann (1935) is better in modeling granular drag force. Later, using this relation granular viscosity of fluidized bed is calculated. At the end, network of force chains is compared for fluidized and packed bed and observed that for packed bed network of force chain increases with the depth of intrusion. However, for fluidized bed the network of force chain breaks due to passing gas resulting in depth independent granular drag force.

ACKNOWLEDGEMENTS

Author would like to acknowledge Higher education Commission (HEC) Pakistan for providing financial assistance. The author also likes to show gratitude for fruitful discussions on fluidization by Professor Junfeng Zhang of Laurentian University, Canada.

REFERENCES

Jaeger, H. M., S. R. Nagel, and R. P.Behringer (1996). Granular solids, liquids, and gases. *Reviews of Modern Physics* 68(4), 1259-1273.

Yang, W. C. (2003), *Handbook of fluidization and fluid-particle systems*, CRC press.

Le Guen, L., F. Huchet, and P. Tamagny (2011). Drying and heating modelling of granular flow:

application to the mix-asphalt processes. *Journal of Applied Fluid Mechanics* 4(2), pp 71-80.

Ottino, J. M., and D. V. Khakhar (2000). Mixing and segregation of granular materials. *Annu Rev Fluid Mech* 32, 55-91.

Behringer, R. P. (2015). Jamming in granular materials. *Comptes rendus - Physique*16(1), 10-25.

Nirmala, G., and L. Muruganandam (2015). An Experimental Study of Liquid-Solid Flow in a Circulating Fluidized Bed of Varying Liquid Viscosity. *Journal of Applied Fluid Mechanics* 8(1).

Conway, S. L., T. Shinbrot, and B. J. Glasser (2004). A Taylor vortex analogy in granular flows. *Nature* 431(7007), 433-437.

Walsh, A. M., K. E. Holloway, P. Habdas, and J. R. de Bruyn (2003). Morphology and scaling of impact craters in granular media. *Physical Review Letters* 91(10).

Uehara, J. S., M. A. Ambroso, R. P. Ojha, and D. J. Durian (2003). Low-speed impact craters in loose granular media. *Physical Review Letters* 90(19).

Crassous, J., D. Beladjine, and A. Valance (2007). Impact of a projectile on a granular medium described by a collision model. *Physical Review Letters* 99(24).

Clark, A. H., L. Kondic, and R. P. Behringer (2012). Particle Scale Dynamics in Granular Impact. *Physical Review Letters* 109(23).

Lohse, D., R. Rauhe, R. Bergmann, D. and van der Meer (2004). Creating a dry variety of quicksand. *Nature* 432(7018), 689-690.

Peng, Z., X. T. Xu, K. Q. Lu, and M. Y. Hou (2009). Depth dependence of vertical plunging force in granular medium. *Physical Review E* 80(2).

Hill, G., S. Yeung, and S. A. Koehler (2005). Scaling vertical drag forces in granular media. *Europhys Lett* 72(1), 137-143.

Katsuragi, H., and D. J. Durian (2007). Unified force law for granular impact cratering. *Nature Physics* 3(6), 420-423.

Hou, M., Z. Peng, R. Liu, Y. Wu, Y. Tian, K. Lu, and C. K. Chan (2005). Projectile impact and penetration in loose granular bed. *Science and Technology of Advanced Materials* 6(7), 855-859.

Clark, A. H., A. J. Petersen, and R. P. Behringer (2014). Collisional model for granular impact dynamics. *Physical Review E* 89(1).

Lim, K. S., and P. K. Agarwal (1994). Circulatory Motion of a Large and Lighter Sphere in a Bubbling Fluidized-Bed of Smaller and Heavier Particles. *Chemical Engineering Science* 49(3), 421-424.

Rios, G. M., K. D. Tran, and H. Masson (1986). Free Object Motion in a Gas-Fluidized Bed. *Chemical Engineering Communications* 47(4-6), 247-272.

Cundall, P. A., and O. D. L. Strack (1979). Discrete Numerical-Model for Granular Assemblies. *Geotechnique* 29(1), 47-65.

Sulsky, D., S. J. Zhou, and H. L. Schreyer (1995). Application of a particle-in-cell method to solid mechanics. *Computer physics communications* 87(1-2), 236-252.

Anderson, T. B., and R. Jackson (1967). A Fluid Mechanical Description of Fluidized Beds. *Ind Eng Chem Fund* 6(4), 527-539.

Tsuji, Y., T. Kawaguchi, and T. Tanaka (1993). Discrete particle simulation of two-dimensional fluidized bed. *Chemical Engineering Science* 77(1), 79-87.

Patankar, S. V. (1980). Numerical Heat Transfer And Fluid Flow. *Numerical Heat Transfer And Fluid Flow*, 1-197.

Zaidi, A. A. (2018). Study of particle inertia effects on drag force of finite sized particles in settling process. *Chemical Engineering Research and Design* 132, 714-728.

Zaidi, A. A. (2018). Particle velocity distributions and velocity fluctuations of non-Brownian settling particles by particle-resolved direct numerical simulation. *Physical Review E* 98(5), 053103.

Zaidi, A. A., T. Tsuji, and T. Tanaka (2015). Direct numerical simulations of inertial settling of non-Brownian particles. *Korean Journal of Chemical Engineering* 32(4), 617-628.

Zaidi, A. A. (2018). Particle resolved direct numerical simulation of free settling particles for the study of effects of momentum response time on drag force. *Powder Technology* 335, 222-234.

Ishibashi, I., C. Perry III, and T. K. Agarwal (1994). Experimental determinations of contact friction for spherical glass particles. *Soils and foundations* 34(4), 79-84.

Sondergaard, R., K. Chaney, and C. Brennen (1990). Measurements of solid spheres bouncing off flat plates. *Journal of Applied Mechanics* 112(3), 694-699.

Li, L., and B. Li (2018). Implementation and validation of a volume-of-fluid and discrete-element-method combined solver in OpenFOAM. *Particuology* 39, 109-115.

Li, L., B. Li, and Z. Liu (2017). Modeling of spout-fluidized beds and investigation of drag closures using OpenFOAM. *Powder Technology* 305, 364-376.

Wen, C. Y., and Y. H. Yu (1966). Mechanics of fluidization. *Chemical Engineering Progress Symposium Series* 62, 100–111.

Xu, Y., J. T. Padding, and J. A. M. Kuipers (2014). Numerical investigation of the vertical plunging force of a spherical intruder into a prefluidized granular bed. *Physical Review E* 90(6).

Stone, M., R. Barry, D. Bernstein, M. Pelc, Y. Tsui, and P. Schiffer (2004). Local jamming via penetration of a granular medium. *Physical Review E* 70(4), 041301.

Schiller, L., and Z. Naumann(1935). A Drag Coefficient Corre-lation. *VDI Zeitung* 77(8), 318-320.

Grace, J. R. (1970). The viscosity of fluidized beds. *Chemical Engineering Research and Design* 48(A10), 30-33.

Schugerl, K., M. Merz, and F. Fetting (1961). Rheologische Eigenschaften Von Gasdurchstromten Fliessbettsystemen. *Chemical Engineering Science* 15(1-2), 1-38.

Zaidi, A. A. (2018). Particle velocity distributions and velocity fluctuations of non-Brownian settling particles by particle-resolved direct numerical simulation. *Physical Review* E 98(5), 053103.